Fan *et al. Satellite Navigation* (2023) 4:27
https://doi.org/10.1186/s43020-023-00117-2

Satellite Navigation
https://satellite-navigation.springeropen.com/

ORIGINAL ARTICLE

Open Access

A double sideband combined tracking method for Galileo E5 AltBOC signals

Tongwen Fan[1], Tisheng Zhang[1*], Hongping Zhang[1], Jun Mo[2] and Xiaoji Niu[1,3]

Abstract

The Galileo navigation satellite system (Galileo) E5 Alternative Binary Offset Carrier (AltBOC) signal brings various challenges due to its complex modulation, wide bandwidth, and multi-peaked auto-correlation function. While wideband tracking needs to solve the ambiguity problem and design dedicated baseband channels, the single-sideband cannot have the outstanding performance of the AltBOC signal. We propose a new tracking method called "Double Sideband Combined Tracking" (DSCT), which can fully exploit the AltBOC signal's code tracking accuracy without ambiguity and ensure compatibility with Binary Phase Shift Keying (BPSK) processing channels, easily implemented in hardware. The DSCT employs one phase locked loop and one delay locked loop to track the carrier and code, respectively. The double-sideband correlation results used by the two loops are recovered by coherently combining the single-sideband correlation results of the two BPSK channels. Meanwhile, the combined model, the loop discriminator, and the ambiguity detection of the DSCT are discussed. Furthermore, the code tracking error caused by thermal noise is modeled and analyzed. The test results based on real Galileo E5 signals show that the DSCT exhibits better or comparable code tracking accuracy to the AltBOC wideband tracking method. When the loop falsely locks onto a side-peak, the DSCT can quickly detect and re-lock on the main peak.

Keywords Galileo E5, Alternative binary offset carrier, Tracking loop, Unambiguous tracking, Double-sideband tracking

Introduction

The Galileo navigation satellite system (Galileo) E5 signal has the most complex structure among all Galileo signals. It uses an Alternative Binary Offset Carrier (AltBOC) modulation, which combines four signal components into a constant envelope signal. The spectrum of the Galileo E5 signal spreads over two adjacent frequency bands, E5a and E5b. While the E5 signal has a bandwidth of 51.15 MHz, the bandwidths of E5a and E5b are 20.46 MHz with 30.69 MHz apart. The sharp main peak of the AltBOC signal's Auto-Correlation Function (ACF) can bring great code tracking (Diessongo et al., 2014) and anti-multipath performance (Prochniewicz & Grzymala, 2021; Silva et al., 2012; Xiao et al., 2018; Ye et al., 2017). However, due to the multiple side-peaks in the ACF, the tracking loop may falsely lock onto a side-peak, which is called the ambiguous problem (Lee et al., 2009).

The tracking methods for the advanced but complex AltBOC signal can mainly be divided into two categories: the upper/lower Single-Sideband modulation (SSB) independent tracking and the wideband tracking. A Binary Phase-Shift Keying like (BPSK-like) method to track Binary Offset Carrier (BOC) signals was proposed, which is also applicable to AltBOC signals (Burian et al., 2006; Kovár et al., 2011; Martin et al., 2003). In the BPSK-like method, the upper or lower sideband of the AltBOC signal is tracked as a BPSK signal, and a BPSK ACF is obtained. The tracking loop structure of the BPSK-like method is simple and compatible with the common

*Correspondence:
Tisheng Zhang
zts@whu.edu.cn
[1] GNSS Research Center, Wuhan University, Wuhan 430072, China
[2] GLOBSKY Technology Inc., San Jose, CA, USA
[3] Hubei Luojia Laboratory, Wuhan 430072, China

baseband processing channel of the BPSK signal. However, this method sacrifices the outstanding code tracking and anti-multipath performance of the AltBOC signal (Shivaramaiah et al., 2009).

An ACF-based wideband tracking method for AltBOC signals was proposed (Shivaramaiah & Dempster, 2009a; Sleewaegen et al., 2004), which evaluates the ACF of the wideband AltBOC signal. It employs the local early, prompt, and late replicas of the AltBOC signal to correlate with the received AltBOC signal. The ACF-based method can achieve the full potential of the AltBOC signal in code tracking and anti-multipath. However, this method has an ambiguity problem and requires the baseband processing channels need to be designed specially. Several wideband tracking methods were proposed to address the ambiguity problem in AltBOC signal tracking, including Side-peaks Cancellation (SC) techniques such as sub-carrier phase cancellation (Heiries et al., 2004; Shivaramaiah & Dempster, 2008) and pseudo correlation function (Chen et al., 2013; Ren et al., 2014; Yao et al., 2010). The fundamental concept of SC techniques involves using a Cross-Correlation Function (CCF) without side-peaks by combining the correlation results of a designed local signal with the AltBOC signal. The Dual Estimate Tracking (DET), initially studied for BOC (Hodgart & Blunt, 2007; Hodgart & Simons, 2012; Hodgart et al., 2007), was also proposed for AltBOC signal tracking (Ren et al., 2012). The DET employs a Phase Locked Loop (PLL), Sub-carrier Locked Loop (SLL), and Delay Locked Loop (DLL) to track the carrier, sub-carrier, and ranging code, respectively. The DET can obtain an unambiguous and accurate code by combining the ranging code and sub-carrier estimates. Although the above methods can solve the ambiguity problem of the AltBOC signal tracking, they need to generate multi-value code signals and their structures greatly differ from the common BPSK channels. Therefore, the above methods need dedicated baseband processing channels, which increases baseband complexity and hardware consumption.

Coherently combining the up and down sidebands of signals for wideband signal tracking was studied. Zhu et al. (2015) proposed the Dual BPSK Tracking (DBT) for AltBOC signals. This method employs sideband correlators, which are compatible with the BPSK's, and coherently combines them to track the carrier, ranging code, and sub-carrier independently via a PLL, DLL and SLL, respectively. Subsequently, Feng et al. (2016) proposed an unambiguous BOC tracking method using a coherent combination of dual sidebands. This approach requires four complex correlators to track the carrier, ranging code, and sub-carrier independently. Borio (2017) proposed a Coherent Sideband (CSB) approach for BOC signals. The CSB employs sideband processing on the two main lobes of the BOC spectrum separately and realizes the independent tracking of the carrier, ranging code, and sub-carrier. These methods based on coherently combining sidebands can obtain an unambiguous and accurate estimate, while their correlator architecture is compatible with the BPSK's. However, these methods track the carrier, sub-carrier, and ranging code independently, and need three discriminators and loop filters.

We proposed a novel AltBOC tracking method, namely Double Sideband Combined Tracking (DSCT). Unlike the coherently combining sidebands tracking method mentioned above, the DSCT combines double sideband correlation results to jointly track sub-carrier and code via a DLL. Consequently, this method has a simpler loop structure. The contributions mainly include:

First, the double sideband combined tracking for AltBOC signal tracking is discussed, which is a simple loop structure and compatible with the BPSK's correlators.

Second, the code tracking error model of the DSCT caused by thermal noise is established, which is used for loop parameter design.

Third, the code tracking performance of the DSCT is tested and compared with BPSK-like, ACF-Based and DBT methods using real Galileo E5 signals.

The remainder of this paper is organized as follows. First, the structure and characteristics of the AltBOC signal are described. Next, an accurate, unambiguous, and compatible DSCT method is proposed. Then, the code tracking error caused by the thermal noise of the DSCT is modeled and analyzed. After that, using the real static Galileo E5 signal, the performance of the proposed DSCT is tested and discussed. Finally, conclusions and future work are summarized.

Galileo E5 signal model

The Galileo E5 signal employs the AltBOC modulation with a carrier frequency of 1191.795 MHz, a sub-carrier frequency of 15.345 MHz, and a code chipping rate of 10.23 MHz. Due to the complex sub-carriers, Galileo E5 signal spectrum includes a lower side lobe E5a centered at 1176.45 MHz and an upper side lobe E5b centered at 1207.14 MHz. The E5 signal can be approximated as two separate QPSK/BPSK signals modulated on the E5a sideband and E5b sideband, respectively (Padokhin et al., 2021; Rebeyrol et al., 2007). The E5 baseband signal can be expressed as (European Union, 2021):

$$
\begin{aligned}
s_{\mathrm{E5}}(t) = & \frac{1}{2\sqrt{2}}\left(e_{\mathrm{E5a}-I}(t) + \mathrm{j}e_{\mathrm{E5a}-Q}(t)\right)\left[s_{\mathrm{sc,s}}(t) - \mathrm{j}s_{\mathrm{sc,s}}\left(t - \frac{T_{\mathrm{sc}}}{4}\right)\right] \\
& + \frac{1}{2\sqrt{2}}\left(e_{\mathrm{E5b}-I}(t) + \mathrm{j}e_{\mathrm{E5b}-Q}(t)\right)\left[s_{\mathrm{sc,s}}(t) + \mathrm{j}s_{\mathrm{sc,s}}\left(t - \frac{T_{\mathrm{sc}}}{4}\right)\right] \\
& + \frac{1}{2\sqrt{2}}\left(\bar{e}_{\mathrm{E5}a-I}(t) + \mathrm{j}\bar{e}_{\mathrm{E5a}-Q}(t)\right)\left[s_{\mathrm{sc,p}}(t) - \mathrm{j}s_{\mathrm{sc,p}}\left(t - \frac{T_{\mathrm{sc}}}{4}\right)\right] \\
& + \frac{1}{2\sqrt{2}}\left(\bar{e}_{\mathrm{E5b}-I}(t) + \mathrm{j}\bar{e}_{\mathrm{E5b}-Q}(t)\right)\left[s_{\mathrm{sc,p}}(t) + \mathrm{j}s_{\mathrm{sc,p}}\left(t - \frac{T_{\mathrm{sc}}}{4}\right)\right]
\end{aligned} \tag{1}
$$

$e_{\mathrm{E5X}-Y}$ denotes the binary signal component called "single signal", where $X{=}a, b$ represents that the signal is modulated on the E5a or E5b sideband, and $Y{=}I, Q$ represents whether the signal is in-phase or quadrature-phase modulated. The in-phase single signals carry navigation data, called "data component". And the quadrature-phase single signals are data-less, called "pilot component". The dashed terms $\bar{e}_{\mathrm{E5X}-Y}(\mathrm{X} = \mathrm{a},\ \mathrm{b};\ Y = I, Q)$ called "product signals", can realize a constant envelop modulation which is beneficial to the transmission of the signal (Changlu et al., 2010). $s_{\mathrm{sc,s}}$ and $s_{\mathrm{sc,p}}$ are the four-level sub-carriers of the single and product signals, respectively, and T_{sc} denotes the sub-carrier period.

The AltBOC sub-carrier for the single signals only has harmonics at $+f_{\mathrm{sc}}$, $-7f_{\mathrm{sc}}$, and $+9f_{\mathrm{sc}}$, while the sub-carrier for the product signals only has harmonics at $-3f_{\mathrm{sc}}$, and $+5f_{\mathrm{sc}}$ (Lestarquit et al., 2008). Considering the radio frequency bandwidth for the Galileo E5 signal is below 90 MHz, the intermodulation product at $\pm 3f_{\mathrm{sc}}$, $\pm 5f_{\mathrm{sc}}$ is filtered out mostly, and only the fundamental harmonic of the sub-carrier can be received. Therefore, the AltBOC signal received can be approximated as the Alternative Linear Offset Carrier (AltLOC) signal, written as (Shivaramaiah & Dempster, 2009b):

$$
\begin{aligned}
s_{\mathrm{AL}}(t) = & \left[e_{\mathrm{E5a}-I}(t) + \mathrm{j}e_{\mathrm{E5a}-Q}(t)\right]\exp\left(-\mathrm{j}2\pi f_{\mathrm{sc}}t\right) \\
& + \left[e_{\mathrm{E5b}-I}(t) + \mathrm{j}e_{\mathrm{E5b}-Q}(t)\right]\exp\left(\mathrm{j}2\pi f_{\mathrm{sc}}t\right)
\end{aligned} \tag{2}
$$

Hence, the AltBOC signal can be tracked using an AltLOC replica. While the AltBOC signal's pilot component is normally employed for tracking, the data component is for data demodulation. For the pilot component tracking, the local AltLOC replica can be written as:

$$
\begin{aligned}
s_{\mathrm{AL}}(t) &= e_{\mathrm{E5a}}(t)\exp\left(-\mathrm{j}2\pi f_{\mathrm{sc}}t\right) + e_{\mathrm{E5b}}(t)\exp\left(\mathrm{j}2\pi f_{\mathrm{sc}}t\right) \\
&= s_{\mathrm{E5a}}(t) + s_{\mathrm{E5b}}(t)
\end{aligned} \tag{3}
$$

where e_{E5a} and e_{E5b} are the binary ranging codes of E5a and E5b sidebands, respectively. The ACF of the AltBOC(15,10) signal (Yarlykov, 2016), the CCF between AltBOC and AltLOC, and the correlation function generated by the BPSK-Like method (Margaria et al., 2008) are depicted in Fig. 1.

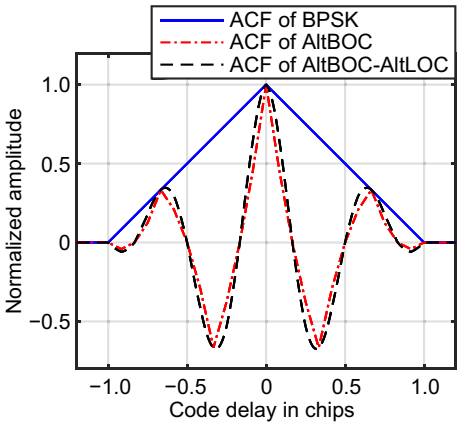

Fig. 1 Correlation functions

From Fig. 1, it can be seen that the AltBOC-AltLOC CCF and the AltBOC ACF curve almost coincide. Therefore, to reduce the implementation complexity of the local signal generator, the AltBOC signal can be tracked with an AltLOC local replica (De Wilde et al., 2004; Sleewaegen et al., 2004). However, the two correlation function curves have more than one peak, which causes the ambiguity problem. In comparison, the BPSK-Like method generates a correlation function that only has a main peak without any false lock points but loses the narrow peak of the AltBOC ACF.

Double sideband combined tracking method

In this section, the DSCT structure is proposed, and a combination model is derived that can obtain the Double-Sideband (DSB) correlation result from the upper and lower SSB correlation results. Then, the DSCT loop discriminator and the ambiguity detection are described.

Structure of the DSCT

The DSCT structure is shown in Fig. 2. It consists of two BPSK processing channels on the left side, which are implemented in hardware. The right side includes the correlation combiners, discriminators, filters, and NCO controller, which can run on software. The correlation combiners and two BPSK channels are the key parts of the DSCT. While the two BPSK channels are compatible with the conventional BPSK loop, and the correlation combiners can combine the upper and lower SSB correlation results into DSB correlation results for code and carrier discriminations.

To obtain the SSB correlation results two BPSK channels are employed to track the lower and upper sidebands of the AltBOC signal, respectively. In the E5a sideband (upper sideband), the cosine and sine carrier replicas are generated with carrier NCO controlling, and the I,Q

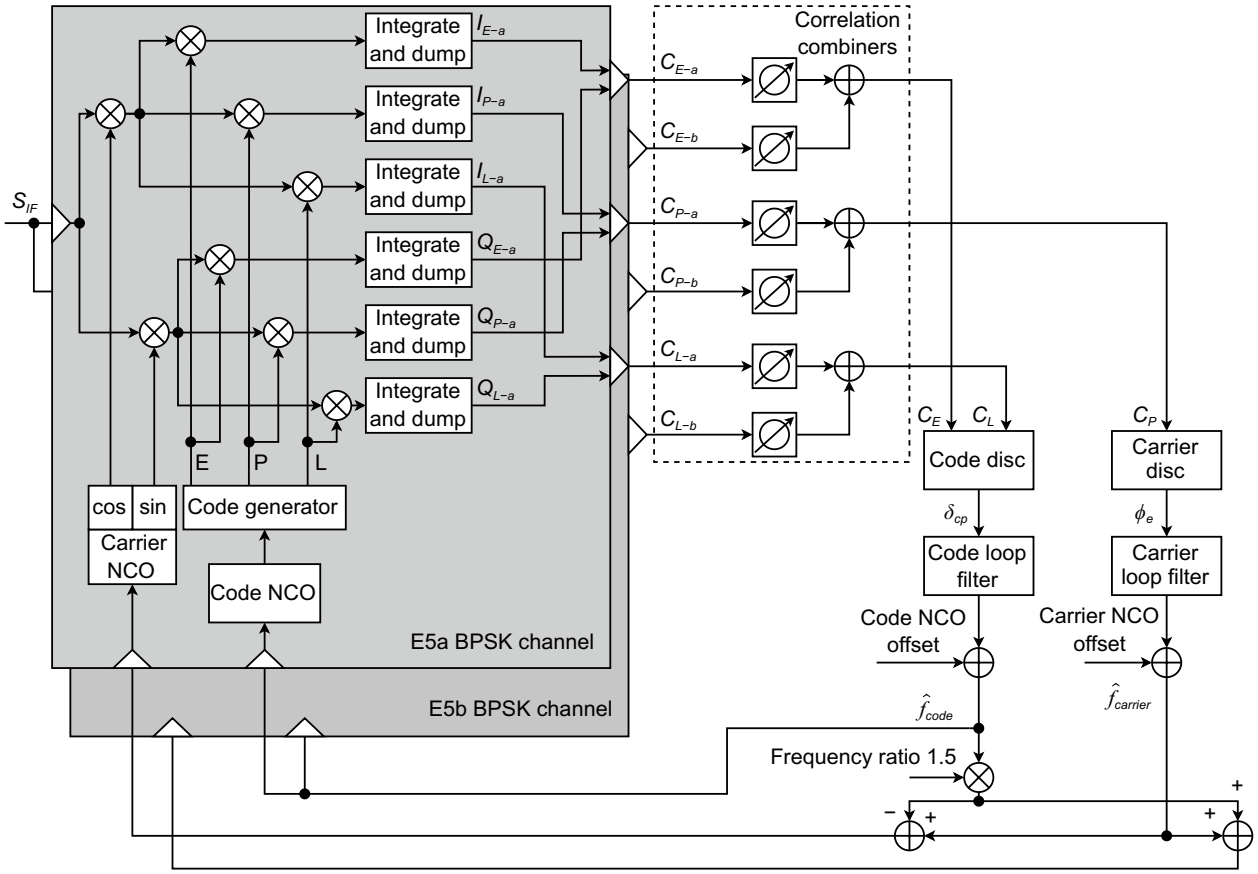

Fig. 2 Structure of the double-sideband combined tracking loop

components can be obtained by multiplying them with the received signal. Then, the *I*,*Q* components are correlated with early, prompt, and late local E5a ranging code replicas. After integration and dump, the six correlation results are output, denoted by I_{E-a}, I_{P-a}, I_{L-a}, Q_{E-a}, Q_{P-a} and Q_{L-a}. Similarly, E5b sideband six correlation results can be obtained, denoted by I_{E-b}, I_{P-b}, I_{L-b}, Q_{E-b}, Q_{P-b} and Q_{L-b}.

Based on the fact that the SSB correlation results contain the DSB phase information, the correlation combiner coherently uses twelve correlation results from the E5a and E5b sidebands to obtain three delayed (early, prompt, and late) complex DSB correlation results C_E, C_P and C_L. The relationship model between SSB and DSB correlation results will be detailed in the next section. Subsequently, C_E and C_L are sent to the DLL discriminator to estimate the code phase error δ_{cp}, which is fed into the code loop filter. The filter output is added with the offset of the code NCO to obtain the local code frequency $\hat{f}_{code}$, which controls the code NCO of the upper and lower sidebands. Meanwhile, the carrier discriminator calculates the carrier phase error ϕ_e based on the prompt DSB correlation result C_P, and ϕ_e is fed into the carrier loop filter. The local carrier frequency $\hat{f}_{carrier}$ can be obtained by adding the carrier loop filter output to the carrier NCO offset.

Though the correlator architecture of DSCT is similar to the sideband coherent combination tracking methods mentioned previously, such as DBT, the essential difference lies in the processing of the correlation results. DSCT obtains a discrimination curve for the DLL by shifting the phases of the early and late correlation results and coherently combining them. However, DBT combines the prompt correlation results for sub-carrier tracking, and the early and late correlation results for code tracking, to obtain a measurement by combining the code and sub-carrier measurements. In comparison, DSCT tracks the AltBOC signals with only a PLL and DLL and does not require an extra SLL for sub-carrier tracking, nor does it need to combine the measurements. The proposed DSCT has following advantages:

1. The hardware processing channels of the DSCT structure are compatible with the BPSK tracking structure. Without a dedicated design, the receiver with BPSK channels can track AltBOC signals via a

PLL and DLL. Therefore, the DSCT can reduce the hardware design complexity and hardware consumption.

2. The DSCT can switch between SSB and DSB tracking modes by using SSB correlation results and DSB correlation results, respectively. During the pull-in stage, the SSB tracking mode can be used for unambiguous tracking. During the tracking stage, the DSB tracking mode can be employed for high-accuracy pseudo-range measurements.

Model of double sideband combination

The relationship between the SSB and AltLOC DSB correlation results can be expressed as (Mo et al., 2021):

$$\begin{cases} C_{\mathrm{E}} = \exp\left(\mathrm{j}3\pi\hat{f}_{\mathrm{code}}\Delta/2\right)C_{\mathrm{E}-a} + \exp\left(-\mathrm{j}3\pi\hat{f}_{\mathrm{code}}\Delta/2\right)C_{\mathrm{E}-b} \\ C_{\mathrm{P}} = C_{\mathrm{P}-a} + C_{\mathrm{P}-b} \\ C_{\mathrm{L}} = \exp\left(-\mathrm{j}3\pi\hat{f}_{\mathrm{code}}\Delta/2\right)C_{\mathrm{L}-a} + \exp\left(\mathrm{j}3\pi\hat{f}_{\mathrm{code}}\Delta/2\right)C_{\mathrm{L}-b} \end{cases} \tag{4}$$

where Δ represents the correlator spacings between the early and late correlators. Similarly, a more general combination of single-sideband correlation results can be written as:

$$\begin{cases} C_{\mathrm{E}} = \exp\left(\mathrm{j}\varphi_{\mathrm{E}-a}\right)C_{\mathrm{E}-a} + \exp\left(\mathrm{j}\varphi_{\mathrm{E}-b}\right)C_{\mathrm{E}-b} \\ C_{\mathrm{P}} = \exp\left(\mathrm{j}\varphi_{\mathrm{P}-a}\right)C_{\mathrm{P}-a} + \exp\left(\mathrm{j}\varphi_{\mathrm{P}-b}\right)C_{\mathrm{P}-b} \\ C_{\mathrm{L}} = \exp\left(\mathrm{j}\varphi_{\mathrm{L}-a}\right)C_{\mathrm{L}-a} + \exp\left(\mathrm{j}\varphi_{\mathrm{L}-b}\right)C_{\mathrm{L}-b} \end{cases} \tag{5}$$

The complex correlation results of two sidebands are phase-shifted and combined in (5). To ensure that combined correlation results can be utilized for carrier and code tracking, it is necessary to confirm the relationship between the shifted phases. Assuming the carrier is wiped off, the received AltBOC signal can be approximated as an AltLOC signal for clarity:

$$s(t) \approx e_{\mathrm{E5a}}(t)\exp[-\mathrm{j}2\pi f_{\mathrm{sc}}(t+t_{\mathrm{scd}})] + e_{\mathrm{E5b}}(t)\exp[\mathrm{j}2\pi f_{\mathrm{sc}}(t+t_{\mathrm{scd}})] \tag{6}$$

where t_{scd} denotes the sub-carrier delay relative to the code. Therefore, the CCF between the received signal $s(t)$ and the local signal $s_{\mathrm{E5a}}(t)$ can be expressed as:

$$\begin{aligned} R_{\mathrm{E5a}}(\tau) &= \frac{1}{T_{\mathrm{code}}}\int_0^{T_{\mathrm{code}}} s(t)s^*_{\mathrm{E5a}}(t-\tau)\mathrm{d}t \\ &\approx \frac{T_{\mathrm{code}}-|\tau|}{T_{\mathrm{code}}}\exp\left(-\mathrm{j}2\pi f_{\mathrm{sc}}\tau - \mathrm{j}\beta\right) \end{aligned} \tag{7}$$

where $\beta = 2\pi f_{\mathrm{sc}} t_{\mathrm{scd}}$. Similarly, the CCF between the received signal $s(t)$ and the local signal $s_{\mathrm{E5b}}(t)$ can be expressed as:

$$R_{\mathrm{E5b}}(\tau) \approx \frac{T_{\mathrm{code}}-|\tau|}{T_{\mathrm{code}}}\exp\left(\mathrm{j}2\pi f_{\mathrm{sc}}\tau + \mathrm{j}\beta\right) \tag{8}$$

Assuming the local code phase advance ε relative to the received signal, the present combined correlation result is given by

$$\begin{aligned} C_{\mathrm{P}}(\varepsilon) &= \exp\left(\mathrm{j}\varphi_{\mathrm{P}-a}\right)R_{\mathrm{E5a}}(-\varepsilon) + \exp\left(\mathrm{j}\varphi_{\mathrm{P}-b}\right)R_{\mathrm{E5b}}(-\varepsilon) \\ &\approx \frac{T_{\mathrm{code}}-|\varepsilon|}{T_{\mathrm{code}}}\exp\left(\mathrm{j}\frac{\varphi_{\mathrm{P}-a}+\varphi_{\mathrm{P}-b}}{2}\right)2 \\ &\quad \cos\left(2\pi f_{\mathrm{sc}}\varepsilon - \beta + \frac{\varphi_{\mathrm{P}-a}-\varphi_{\mathrm{P}-b}}{2}\right) \end{aligned} \tag{9}$$

Since the carrier is wiped off, the imaginary part of $C_{\mathrm{P}}(\varepsilon)$ should be zero. In addition, the modulus of $C_{\mathrm{P}}(\varepsilon)$ should achieve its maximum when $\varepsilon = 0$ for optimal carrier phase discrimination performance.

$$\begin{cases} \Im[C_{\mathrm{P}}(\varepsilon)] = 0 \\ \underset{\varepsilon}{\mathrm{argmax}}\,[|C_{\mathrm{P}}(\varepsilon)|] = 0 \end{cases} \tag{10}$$

The early combined correlation result minus the late one can be written as:

$$\begin{aligned} e_s(\varepsilon) &= \exp\left(\mathrm{j}\varphi_{\mathrm{E}-a}\right)R_{\mathrm{E5a}}(-\varepsilon-\Delta/2) \\ &\quad + \exp\left(\mathrm{j}\varphi_{\mathrm{E}-b}\right)R_{\mathrm{E5b}}(-\varepsilon-\Delta/2) \\ &\quad - \exp\left(\mathrm{j}\varphi_{\mathrm{L}-a}\right)R_{\mathrm{E5a}}(-\varepsilon+\Delta/2) \\ &\quad - \exp\left(\mathrm{j}\varphi_{\mathrm{L}-b}\right)R_{\mathrm{E5b}}(-\varepsilon+\Delta/2) \end{aligned} \tag{11}$$

where $e_s(\varepsilon) = C_{\mathrm{E}}(\varepsilon) - C_{\mathrm{L}}(\varepsilon)$. From (7) and (8), $e_s(\varepsilon)$ can be approximated as:

$$\begin{aligned} e_s(\varepsilon) &\approx \frac{T_{\mathrm{code}}-|\varepsilon+\Delta/2|}{T_{\mathrm{code}}}\exp\left(\mathrm{j}\frac{\varphi_{\mathrm{E}-a}+\varphi_{\mathrm{E}-b}}{2}\right)2 \\ &\quad \cos\left(2\pi f_{\mathrm{sc}}\varepsilon - \beta + \frac{\varphi_{\mathrm{E}-a}-\varphi_{\mathrm{E}-b}}{2}\right) \\ &\quad - \frac{T_{\mathrm{code}}-|\varepsilon-\Delta/2|}{T_{\mathrm{code}}}\exp\left(\mathrm{j}\frac{\varphi_{\mathrm{L}-a}+\varphi_{\mathrm{L}-b}}{2}\right)2 \\ &\quad \cos\left(2\pi f_{\mathrm{sc}}\varepsilon - \beta + \frac{\varphi_{\mathrm{L}-a}-\varphi_{\mathrm{L}-b}}{2}\right) \end{aligned} \tag{12}$$

Similar to (10), the imaginary part of $e_s(\varepsilon)$ should be zero. In addition, $e_s(\varepsilon)$ should be an odd function to reflect the code phase error. The above analysis yields:

$$\begin{cases} \Im[e_s(\varepsilon)] = 0 \\ e_s(\varepsilon) = -e_s(-\varepsilon) \end{cases} \tag{13}$$

According to (5), (10) and (13), the combination model of correlation results finally can be expressed as:

$$\begin{cases} C_{\mathrm{E}} = \exp\left(\mathrm{j}\alpha + \mathrm{j}\beta\right) C_{\mathrm{E}-a} + \exp\left(-\mathrm{j}\alpha - \mathrm{j}\beta\right) C_{\mathrm{E}-b} \\ C_{\mathrm{P}} = \exp\left(\mathrm{j}\beta\right) C_{\mathrm{P}-a} + \exp\left(-\mathrm{j}\beta\right) C_{\mathrm{P}-b} \\ C_{\mathrm{L}} = \exp\left(-\mathrm{j}\alpha + \mathrm{j}\beta\right) C_{\mathrm{L}-a} + \exp\left(\mathrm{j}\alpha - \mathrm{j}\beta\right) C_{\mathrm{L}-b} \end{cases} \tag{14}$$

where $\alpha = \varphi_{\mathrm{E}-a} - \beta$. It is important to note that the value of α in (14) is not limited. Therefore, the correlation results can be combined with the different values of α. In addition, (4) is a special case of (14) when $\alpha = 1.5\pi\Delta/T_{\mathrm{code}}$ and $\beta = 0$. The combined correlation results in (14) are equivalent to the correlation results whose local signal is a sum of phase-shifted $s_{\mathrm{E5a}}(t)$ and $s_{\mathrm{E5b}}(t)$. Notably, the equivalent local signals are distinct for early and late correlators.

Loop discriminators

The coherent early minus late envelop code discriminator can be expressed as (Kaplan & Hegarty, 2017):

$$D_{\mathrm{code}}(\varepsilon) = \Re[C_{\mathrm{E}}(\varepsilon) - C_{\mathrm{L}}(\varepsilon)] \tag{15}$$

Substituting (12) into (15) gives

$$D_{\mathrm{code}}(\varepsilon) = 2\left[\frac{T_{\mathrm{code}} - |\varepsilon + \Delta/2|}{T_{\mathrm{code}}}\cos\left(2\pi f_{\mathrm{sc}}\varepsilon + \alpha\right) - \frac{T_{\mathrm{code}} - |\varepsilon - \Delta/2|}{T_{\mathrm{code}}}\cos\left(2\pi f_{\mathrm{sc}}\varepsilon - \alpha\right)\right] \tag{16}$$

From (16), it can be seen that the shape of the discriminator output curve will change with the change of α. Figure 3 depicts the discriminator outputs as a function of α when $\Delta = 0.5T_{\mathrm{code}}$.

Figure 3 shows that changing the value of α affects the slope of the discriminator's linear region, consequently impacting the thermal noise performance of code phase tracking. Notably, the slope of the linear region almost reaches its maximum when $\alpha = 0.45\pi$, while the linearity region and stability region of the discriminator almost approaches their maximum when $\alpha = 0.9\pi$. The discriminator output curve is similar to a sine curve, which is mainly affected by the sub-carrier. The DBT utilizes a pure PLL discriminator for tracking the sub-carrier, while the DSCT employs a DLL discriminator for tracking both the code and sub-carrier. Consequently, the accuracy of the two methods should be comparable in theory.

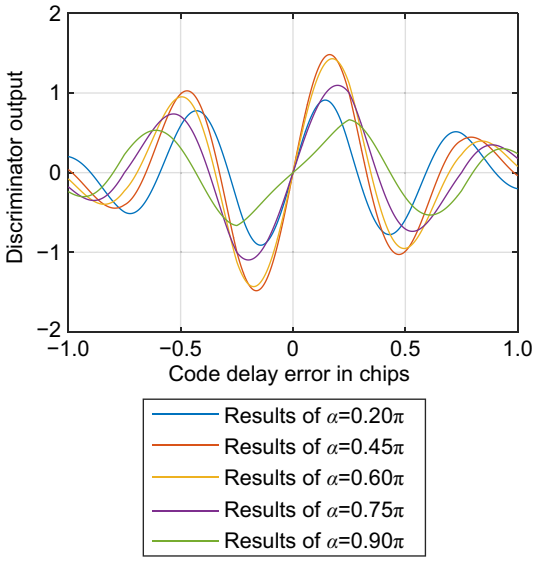

Fig. 3 Discriminator outputs as a function of α

Considering the carrier frequency tracking error, the combined correlation result, derived from (14), is approximately:

$$\begin{aligned} C_{\mathrm{P}}(\varepsilon) \approx{}& \frac{T_{\mathrm{code}} - |\varepsilon|}{T_{\mathrm{code}}} 2\cos\left(2\pi f_{\mathrm{sc}}\varepsilon\right) T_{\mathrm{int}} \\ & \mathrm{sinc}\left(\delta f_{\mathrm{carrier}} T_{\mathrm{int}}\right) \exp\left[\mathrm{j}\left(\pi\delta f_{\mathrm{carrier}} T_{\mathrm{int}} + \delta\theta\right)\right] \end{aligned} \tag{17}$$

where T_{int} is the loop integration time, $\delta f_{\mathrm{carrier}} = f_{\mathrm{carrier}} - \hat{f}_{\mathrm{carrier}}$ is the carrier frequency error, and $\delta\theta = \theta - \hat{\theta}$ is the carrier phase error.

Since the pilot channel is data-less, a pure PLL discriminator is implemented in the carrier tracking loop to obtain a wider pull-in range. The carrier discriminator can be modeled as (Kaplan & Hegarty, 2017):

$$D_{\mathrm{carrier}}(\theta) = \arctan[\Im(C_{\mathrm{P}}), \Re(C_{\mathrm{P}})] \simeq \pi\delta f_{\mathrm{carrier}} T_{\mathrm{int}} + \delta\theta \tag{18}$$

The design of the loop filters in the DSCT is similar to that of the common tracking loop and will not be discussed here (Xie, 2009).

Ambiguity detection

The loop may falsely lock since the discriminator output curve in Fig. 3 has multiple cross-zero points. When a false lock occurs, the tracking error can be reflected in the upper and lower SSB correlation results. The Phase Lock Indication (PLI) can quickly and accurately detect whether the upper and lower sideband carrier phases are tracking correctly. The PLI is defined as (Spilker et al., 1996):

$$\begin{cases} D_{\mathrm{PLI}-a} = \dfrac{[\Re(C_{\mathrm{P}-a})]^2 - [\Im(C_{\mathrm{P}-a})]^2}{[\Re(C_{\mathrm{P}-a})]^2 + [\Im(C_{\mathrm{P}-a})]^2} \\ D_{\mathrm{PLI}-b} = \dfrac{[\Re(C_{\mathrm{P}-b})]^2 - [\Im(C_{\mathrm{P}-b})]^2}{[\Re(C_{\mathrm{P}-b})]^2 + [\Im(C_{\mathrm{P}-b})]^2} \end{cases} \tag{19}$$

In addition, a non-coherent discriminator can detect false locks by obtaining an unambiguous triangular

correlation function from single-sideband correlation results:

$$D_{\text{detect}} = \left(1 - \frac{\Delta}{2}\right) \frac{|C_{\text{E}-a}| + |C_{\text{E}-b}| - |C_{\text{L}-a}| - |C_{\text{L}-b}|}{|C_{\text{E}-a}| + |C_{\text{E}-b}| + |C_{\text{L}-a}| + |C_{\text{L}-b}|} \tag{20}$$

When the false lock occurs, it can be detected by the above two methods quickly and accurately, and the tracking is adjusted from DSB tracking to unambiguous SSB tracking. When the loop re-locks the main peak, the DSB tracking returns to work.

Thermal noise model

To analyze the code tracking performance and guide loop parameter design, the DSCT's code phase error induced by thermal noise is derived and compared with that of other methods. When using a coherent early-late discriminator, the variance of the code phase error induced by thermal noise can be expressed as (Betz & Kolodziejski, 2009):

$$\sigma^2_{\text{CELP}} = \frac{B_{\text{L}}(1 - 0.5B_{\text{L}}T)\int_{-\beta_{\text{r}}/2}^{\beta_{\text{r}}/2} G_s(f)\sin^2(\pi f\Delta)\,\text{d}f}{(2\pi)^2 C_s/N_0\left[\int_{-\beta_{\text{r}}/2}^{\beta_{\text{r}}/2} fG_s(f)\sin(\pi f\Delta)\text{d}f\right]^2} \tag{21}$$

where B_{L} is the equivalent noise bandwidth of the code tracking loop, T is the pre-detection integration time, β_{r} is the two-sided bandwidth of the receiver front-end, and $G_s(f)$ is defined as the normalized Power Spectral Density (PSD) of the signal. Since the equivalent local signals of the DSCT's early and late correlators are different, the code phase error cannot be obtained from (21). The variance of the DSCT's code phase error induced by thermal noise can be expressed as (22), as detailed in the Appendix.

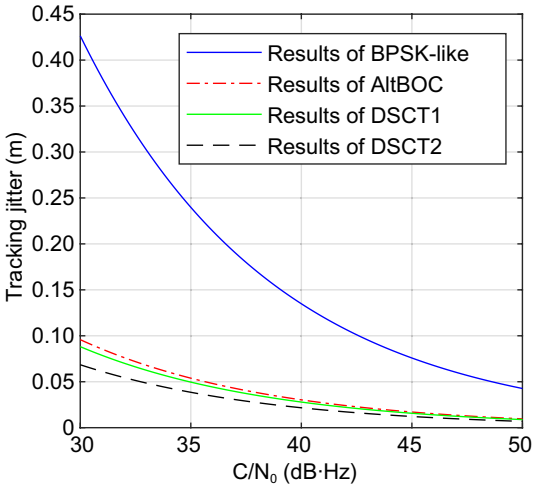

Fig. 4 Theoretical code tracking error caused by thermal noise

method), DSCT1 (with $\alpha = 0.75\pi$), and DSCT2 (with $\alpha = 0.45\pi$) when $B_{\text{L}} = 0.4$Hz, $T = 10$ms, $\beta_{\text{r}} = 56$MHz, $\Delta = 0.5T_{\text{code}}$. The code tracking error of AltBOC is much smaller than that of BPSK, consistent with the theory of the AltBOC signal. The local signal of the DSCT with $\alpha = 0.75\pi = 1.5\pi\Delta/T_{\text{code}}$ is equivalent to the AltLOC signal, which is similar to the AltBOC signal when $\beta_{\text{r}} = 56$MHz. Consequently, the DSCT1 has almost the same code tracking error as that of the AltBOC. Furthermore, the code phase error of the DSCT2 is smaller than those of the AltBOC and DSCT1. Therefore, the model analysis of the code tracking error shows that the code tracking accuracy of the DSCT with an appropriate choice of α surpasses that of the ACF-Based method, and is much better than that of the BPSK.

$$\sigma^2_{\text{DSCT}} = \frac{B_{\text{L}}(1 - 0.5B_{\text{L}}T)\int_{-\beta_{\text{r}}/2}^{\beta_{\text{r}}/2} \left[G_{\text{E5a}}(f)\sin^2(\pi f\Delta + \varphi) + G_{\text{E5b}}(f)\sin^2(\pi f\Delta - \varphi)\right]\text{d}f}{4\pi^2 C_s/N_0\left[\int_{-\beta_{\text{r}}/2}^{\beta_{\text{r}}/2} fG_{\text{E5,E5a}}(f)\sin(\pi f\Delta + \varphi) + fG_{\text{E5,E5b}}(f)\sin(\pi f\Delta - \varphi)\text{d}f\right]^2} \tag{22}$$

According to the PSD of the BPSK and AltBOC signal (Sousa & Nunes, 2013; Wang et al., 2020), the code phase errors induced by thermal noise for BPSK, and AltBOC can be obtained from (21). The cross-spectral density $G_{\text{E5,E5a}}(f)$ in (22) can be obtained from the Fourier transform of CCF between $s_{\text{E5}}(t)$ and $s_{\text{E5a}}(t)$, and similarly, $G_{\text{E5,E5b}}(f)$ can be obtained. Therefore, the code phase errors for DSCT can be obtained from (22).

Figure 4 shows code phase errors of BPSK, AltBOC (the conventional AltBOC wideband tracking

Field test results

The performances of the DSCT, including code tracking accuracy and ambiguity, were tested using the real Galileo E5 signal in static environments. First, to verify the code tracking accuracy, the DSCT, the BPSK-like, the conventional wideband tracking, and the DBT methods were tested and compared. Then, the ambiguity detection performance of the DSCT was tested when the loop falsely locked on a side-peak.

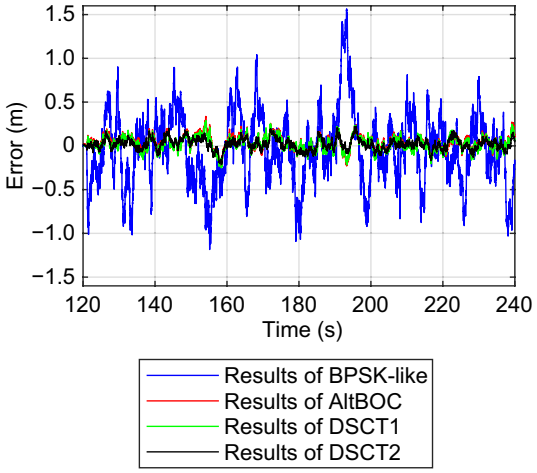

Fig. 5 Code tracking errors of BPSK-like, wideband tracking, and DSCT

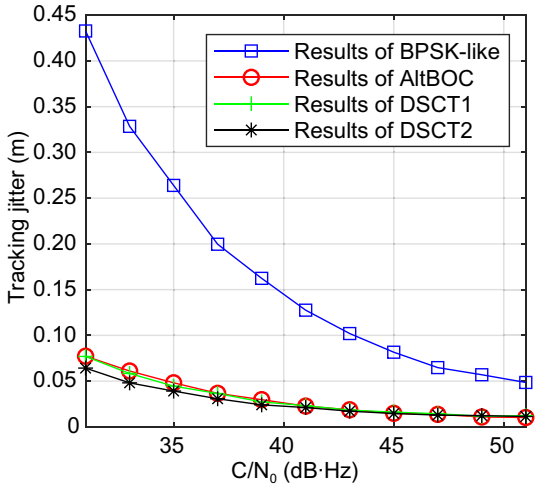

Fig. 6 Measured code tracking jitters of different methods

Table 1 statistical results of code tracking errors

Satellite no.	C/N_0 (dB·Hz)	Tracking jitters of methods (m)			
		BPSK-like	AltBOC	DSCT1	DSCT2
7	31	0.399	0.077	0.077	0.064
21	33	0.293	0.074	0.077	0.059
1	35	0.266	0.058	0.057	0.049
13	39	0.160	0.030	0.030	0.025
31	31	0.458	0.083	0.085	0.072
8	36	0.238	0.045	0.046	0.041
33	34	0.276	0.048	0.046	0.041
26	43	0.085	0.016	0.015	0.015

A LabSat3 Wideband recorder was employed to record Global Navigation Satellite Systems (GNSS) IF data, and the antenna was mounted on the roof. The LabSat3 has a front-end bandwidth of 56 MHz and an *I*,*Q* sampling rate of 58 MHz. In order to test the impact of the thermal noise on the code tracking accuracy, the IF data were polluted with Gaussian white noise. The loop parameters were set as follows: the bandwidth of the carrier loop was 15 Hz, the bandwidth of the code loop was 0.4 Hz, the integration time was 10 ms, and the spacing between the early and late correlators was 0.5 chips.

Tests of code tracking accuracy

The conventional AltBOC wideband tracking method was applied to the IF data prior to the addition of Gaussian white noise to obtain the code delay as the reference. All code tracking errors were then calculated relative to this reference. Figure 5 depicts the code tracking errors of the Pseudo Random Noise (PRN) 7 satellite obtained from the BPSK-like, wideband tracking, and DSCT1, and DSCT2 methods.

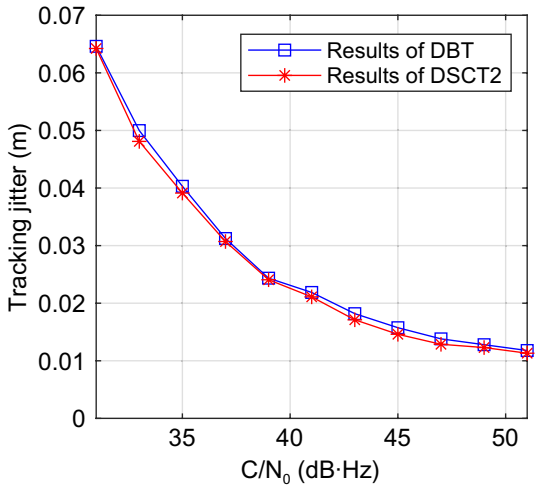

Fig. 7 Code tracking accuracy of the DBT and DSCT

It can be seen that the code tracking errors of the DSCT1 and wideband tracking are relatively close, and slightly worse than that of DSCT2. All three methods have significantly lower code tracking errors than BPSK. The above results are consistent with the theoretical analysis of thermal noise error. The code tracking jitters of different Galileo satellites are listed in Table 1. It can be seen that the accuracies of DSCT1 and AltBOC are similar. On average, DSCT2 is more accurate than AltBOC by 14% and BPSK-like by 83%.

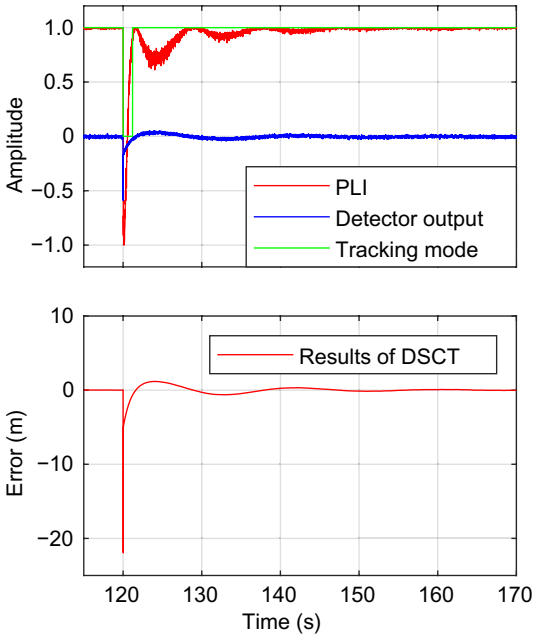

Fig. 8 Ambiguity test results of the DSCT

The code tracking error for the three tracking methods are depicted in Fig. 6. When the carrier-to-noise ratio is in the range of 31 ~ 51 dB·Hz, the proposed method displays a better or comparable accuracy to that of the conventional wideband tracking method, indicating its ability to track the code with high accuracy. In addition, with the increase of the noise power, the performance of the BPSK-like method deteriorates seriously. Comparing Fig. 6 with Fig. 4, the measured code errors are consistent with the theoretical analysis.

In addition, the performances of two combining single sidebands tracking methods, the DBT and the DSCT, are compared in Fig. 7. The measurements of DBT are obtained by combining the code and sub-carrier measurements, while the measurements of DSCT are obtained from the code directly. The results show that when the carrier-to-noise ratio is in the range of 31–51 dB·Hz, the proposed method displays a comparable accuracy to that of the DBT method, which is consistent with the previous analysis. However, the DSCT only needs two track loops to track the AltBOC signals while the DBT needs three.

Test of tracking ambiguity

To test the ambiguity detection performance, the local code delay was manually adjusted to make the loop lock on a side-peak at 120 s. The tracking results of the DSCT are shown in Fig. 8.

Figure 8 presents the ambiguity test results of the DSCT. The top graph shows the minimum value of the PLIs of E5a and E5b sidebands, detector outputs defined in (20), and tracking mode (0 for SSB tracking and 1 for DSB tracking) in the DSCT. The PLI decreases rapidly from around 1, and the detector output deviates rapidly from 0 when the loop is locking on a side-peak. When the PLI is less than 0 and the absolute value of the detector output exceeds 0.25, it indicates that the carrier tracking is incorrect and the code error exceeds the linear range of the discriminator. The DSCT loop then jumps to the main peak based on the detector outputs and switches to SSB tracking. When the PLI exceeds 0.95 and the absolute value of the PLI detector output is below 0.05, it shows that carrier and code tracking accuracy is sufficient for DSB tracking. Consequently, the DSB tracking mode is employed. The bottom graph depicts the code tracking error of the DSCT and shows that the DSCT can re-lock on the main peak when false locks occur.

Conclusions

A new tracking method called DSCT is proposed and implemented for the Galileo E5 AltBOC signal, which can unambiguously track the code with high accuracy and is compatible with BPSK processing channels. In DSCT, the correlation results of the lower and upper AltBOC sidebands are combined to obtain the DSB correlation results, and then the DSB tracking of the AltBOC is implemented. The proposed method displays much better accuracy than the BPSK-like method and the comparable accuracy to the conventional wideband tracking method, as demonstrated by the tests with the real static Galileo E5 signal. In addition, when the loop falsely locks on a side-peak, the DSCT can detect it quickly and make the loop re-lock on the main peak, which solves the ambiguity problem of the AltBOC signal tracking.

Appendix

The correlation results of the DSCT approach are equivalent to those of the early and late correlators for different local signals. Assuming $\beta = 0$, from (14), the equivalent local signals of early and late correlators can be expressed as:

$$\begin{cases} s_{\mathrm{E}}(t) = s_{\mathrm{E5a}}(t)\exp\left(\mathrm{j}\varphi\right) + s_{\mathrm{E5b}}(t)\exp\left(-\mathrm{j}\varphi\right) \\ s_{\mathrm{L}}(t) = s_{\mathrm{E5a}}(t)\exp\left(-\mathrm{j}\varphi\right) + s_{\mathrm{E5b}}(t)\exp\left(\mathrm{j}\varphi\right) \end{cases} \tag{23}$$

where $\varphi = \pi f_{\mathrm{sc}}\Delta - \alpha$. The output of a coherent early-late time-of-arrival (TOA) estimator can be written as (Betz & Kolodziejski, 2009):

$$
\begin{aligned}
e(\varepsilon) = \Re\Bigg\{ & \frac{1}{T}\int_{(k-1)T}^{kT} s_{\mathrm{E5}}(t-t_0)s_{\mathrm{L}}^{*}\Big(t-\tau_s^k-\Delta/2\Big)\mathrm{d}t \\
& -\frac{1}{T}\int_{(k-1)T}^{kT} s_{\mathrm{E5}}(t-t_0)s_{\mathrm{E}}^{*}\Big(t-\tau_s^k+\Delta/2\Big)dt \\
& +\frac{1}{T}\int_{(k-1)T}^{T} w(t)\exp\big(-\mathrm{j}\theta\big)\big[s_{\mathrm{L}}^{*}\big(t-\tau_k^s-\Delta/2\big)-s_{\mathrm{E}}^{*}\big(t-\tau_k^s+\Delta/2\big)\big]\mathrm{d}t\Bigg\}
\end{aligned} \tag{24}
$$

where t_0 is TOA, τ_k^s is smoothed TOA estimate, $w(t)$ is the noise, θ is carrier phase, and $\varepsilon = t_0 - \tau_k^s$. Denote the first two terms in (24) as $e_{\mathrm{L}}(\varepsilon)$ and $e_{\mathrm{E}}(\varepsilon)$, respectively. They can be approximated as (Betz & Kolodziejski, 2009):

According to the cross-correlation theorem, the Cross-Spectral Density (CSD) can be expressed as:

$$
\begin{cases}
e_{\mathrm{L}}(\varepsilon) \approx \Re\Big\{\frac{1}{T}\int_{-\beta_{\mathrm{r}}/2}^{\beta_{\mathrm{r}}/2} S_{\mathrm{E5}}(f)S_{\mathrm{L}}^{*}(f)\exp[\mathrm{j}2\pi f(-\varepsilon+\Delta/2)]\mathrm{d}f\Big\} \\
e_{\mathrm{E}}(\varepsilon) \approx \Re\Big\{\frac{1}{T}\int_{-\beta_{\mathrm{r}}/2}^{\beta_{\mathrm{r}}/2} S_{\mathrm{E5}}(f)S_{\mathrm{E}}^{*}(f)\exp[\mathrm{j}2\pi f(-\varepsilon-\Delta/2)]\mathrm{d}f\Big\}
\end{cases} \tag{25}
$$

where $S_{\mathrm{E5}}(f)$, $S_{\mathrm{L}}(f)$ and $S_{\mathrm{E}}(f)$ are the Fourier transform of $s_{\mathrm{E5}}(t)$, $s_{\mathrm{L}}(t)$ and $s_{\mathrm{E}}(t)$, respectively. Define $e_s(\varepsilon) = e_{\mathrm{L}}(\varepsilon) - e_{\mathrm{E}}(\varepsilon)$, and from (23) and (25) it can be expanded as:

$$
\begin{aligned}
e_s(\varepsilon) &= \Re\Bigg\{\frac{1}{T}\int_{-\beta_{\mathrm{r}}/2}^{\beta_{\mathrm{r}}/2} S_{\mathrm{E5}}(f)\big\{S_{\mathrm{L}}^{*}(f)\exp[\mathrm{j}2\pi f(-\varepsilon+\Delta/2)]-S_{\mathrm{E}}^{*}(f)\exp[\mathrm{j}2\pi f(-\varepsilon-\Delta/2)]\big\}\mathrm{d}f\Bigg\} \\
&= \frac{1}{T}\int_{-\beta_{\mathrm{r}}/2}^{\beta_{\mathrm{r}}/2} S_{\mathrm{E5}}(f)2\sin(2\pi f\varepsilon)\big[S_{\mathrm{E5a}}^{*}(f)\sin(\pi f\Delta+\varphi)+S_{\mathrm{E5b}}^{*}(f)\sin(\pi f\Delta-\varphi)\big]\mathrm{d}f
\end{aligned} \tag{26}
$$

where $S_{\mathrm{E5a}}(f)$ and $S_{\mathrm{E5b}}(f)$ are the Fourier transform of $s_{\mathrm{E5a}}(t)$ and $s_{\mathrm{E5b}}(t)$, respectively. Assuming ε is small, the approximation of $e_s(\varepsilon)$ is

$$
e_s(\varepsilon) \approx \frac{4\pi\varepsilon}{T}\int_{-\beta_{\mathrm{r}}/2}^{\beta_{\mathrm{r}}/2} fS_{\mathrm{E5}}(f)\big[S_{\mathrm{E5a}}^{*}(f)\sin(\pi f\Delta+\varphi)+S_{\mathrm{E5b}}^{*}(f)\sin(\pi f\Delta-\varphi)\big]\mathrm{d}f \tag{27}
$$

$$\begin{cases} G_{\mathrm{E5,E5a}}(f) = \frac{1}{TC_s} S_{\mathrm{E5}}(f) S^*_{\mathrm{E5a}}(f) \\ G_{\mathrm{E5,E5b}}(f) = \frac{1}{TC_s} S_{\mathrm{E5}}(f) S^*_{\mathrm{E5b}}(f) \end{cases} \tag{28}$$

where $G_{\mathrm{E5,E5a}}(f)$ is the CSD between $s_{\mathrm{E5}}(t)$ and $s_{\mathrm{E5a}}(t)$, $G_{\mathrm{E5,E5b}}(f)$ is the CSD between $s_{\mathrm{E5}}(t)$ and $s_{\mathrm{E5b}}(t)$, and C_s is the signal carrier power. Substituting (28) into (27) yields

$$\begin{aligned} e_s(\varepsilon) &\approx 4\pi\varepsilon C_s \int_{-\beta_r/2}^{\beta_r/2} f G_{\mathrm{E5,E5a}}(f) \sin(\pi f \Delta + \varphi) \\ &\quad + f G_{\mathrm{E5,E5b}}(f) \sin(\pi f \Delta - \varphi) \mathrm{d}f \\ &= C_s K \varepsilon \end{aligned} \tag{29}$$

where

$$\begin{aligned} K = 4\pi \int_{-\beta_r/2}^{\beta_r/2} & f G_{\mathrm{E5,E5a}}(f) \sin(\pi f \Delta + \varphi) \\ & + f G_{\mathrm{E5,E5b}}(f) \sin(\pi f \Delta - \varphi) \mathrm{d}f \end{aligned} \tag{30}$$

Given τ_k^s, the conditional variance of unsmoothed TOA estimate τ_k^u can be written as:

$$\mathrm{var}\{\tau_k^u | \tau_k^s\} = \frac{\mathrm{var}\{e(t_0 - \tau_k^s) | \tau_k^s\}}{C_s^2 K^2} \tag{31}$$

The conditional variance $\mathrm{var}\{e(t_0 - \tau_k^s) | \tau_k^s\}$ can be expanded as (Betz & Kolodziejski, 2009):

$$\begin{aligned} \mathrm{var}\{e(t_0 - \tau_k^s) | \tau_k^s\} = \frac{1}{2T^2} \int_{(k-1)T}^{kT} \int_{(k-1)T}^{kT} & R_w(t-u) \left[s_{\mathrm{L}}^*\left(t - \tau_s^k - \Delta/2\right) - s_{\mathrm{E}}^*\left(t - \tau_s^k + \Delta/2\right) \right] \\ & \times \left[s_{\mathrm{L}}\left(u - \tau_s^k - \Delta/2\right) - s_{\mathrm{E}}\left(u - \tau_s^k + \Delta/2\right) \right] \mathrm{d}t \mathrm{d}u \end{aligned} \tag{32}$$

where $R_w(\gamma) = E\{w(t) w^*(t-\gamma)\}$ is the autocorrelation of $w(t)$. Similar to (25), (32) can be approximated as:

$$\mathrm{var}\{e(t_0 - \tau_k^s) | \tau_k^s\} \approx \frac{1}{2T^2} \int_{-\beta_r/2}^{\beta_r/2} G_w(f) \left| S_{\mathrm{L}}^*(f) \exp[\mathrm{j}2\pi f(-\varepsilon + \Delta/2)] - S_{\mathrm{E}}^*(f) \exp[\mathrm{j}2\pi f(-\varepsilon - \Delta/2)] \right|^2 \mathrm{d}f \tag{33}$$

where $G_w(f)$ denotes the PSD of $w(t)$. Substituting (23) into (33) gives:

$$\begin{aligned} \mathrm{var}\{e(t_0 - \tau_k^s) | \tau_k^s\} &\approx \frac{2}{T^2} \int_{-\beta_r/2}^{\beta_r/2} G_w(f) \left[|S_{\mathrm{E5a}}(f)|^2 \sin^2(\pi f \Delta + \varphi) + |S_{\mathrm{E5b}}(f)|^2 \sin^2(\pi f \Delta - \varphi) \right] \mathrm{d}f \\ &= \frac{2C_s}{T} \int_{-\beta_r/2}^{\beta_r/2} G_w(f) \left[G_{\mathrm{E5a}}(f) \sin^2(\pi f \Delta + \varphi) + G_{\mathrm{E5b}}(f) \sin^2(\pi f \Delta - \varphi) \right] \mathrm{d}f \end{aligned} \tag{34}$$

where $G_{\mathrm{E5a}}(f)$ and $G_{\mathrm{E5b}}(f)$ are the PSD of $s_{\mathrm{E5a}}(t)$ and $s_{\mathrm{E5b}}(t)$, respectively. From (30), (31) and (34), the conditional variance of unsmoothed TOA estimate is

$$\sigma_u^2 = \mathrm{var}\left\{\tau_k^u \middle| \tau_k^s\right\} \approx \frac{\int_{-\beta_r/2}^{\beta_r/2} G_w(f)\left[G_{\mathrm{E5a}}(f)\sin^2(\pi f\Delta+\varphi) + G_{\mathrm{E5b}}(f)\sin^2(\pi f\Delta-\varphi)\right]\mathrm{d}f}{8\pi^2 TC_s\left[\int_{-\beta_r/2}^{\beta_r/2} fG_{\mathrm{E5,E5a}}(f)\sin(\pi f\Delta+\varphi) + fG_{\mathrm{E5,E5b}}(f)\sin(\pi f\Delta-\varphi)\mathrm{d}f\right]^2} \tag{35}$$

The relationship between the smoothed and unsmoothed estimates of TOA estimates is approximately (Betz & Kolodziejski, 2009)

$$\sigma_s^2 \approx \sigma_u^2 2B_{\mathrm{L}}T(1-0.5B_{\mathrm{L}}T) \tag{36}$$

Therefore, from (35) and (36), and assuming $G_w(f) = N_0$, the variance of DSCT's code phase error induced by thermal noise is

$$\sigma_{\mathrm{DSCT}}^2 \approx \frac{B_{\mathrm{L}}(1-0.5B_{\mathrm{L}}T)\int_{-\beta_r/2}^{\beta_r/2}\left[G_{\mathrm{E5a}}(f)\sin^2(\pi f\Delta+\varphi) + G_{\mathrm{E5b}}(f)\sin^2(\pi f\Delta-\varphi)\right]\mathrm{d}f}{4\pi^2 C_s/N_0\left[\int_{-\beta_r/2}^{\beta_r/2} fG_{\mathrm{E5,E5a}}(f)\sin(\pi f\Delta+\varphi) + fG_{\mathrm{E5,E5b}}(f)\sin(\pi f\Delta-\varphi)\mathrm{d}f\right]^2} \tag{37}$$

Abbreviations

ACF	Auto-correlation function
AltLOC	Alternative linear offset carrier
BOC	Binary offset carrier
BPSK	Binary phase-shift keying
CCF	Cross-correlation function
CSB	Coherent sideband
CSD	Cross-spectral density
DBT	Dual BPSK tracking
DET	Dual estimate tracking
DLL	Delay locked loop
DSB	Double-sideband
DSCT	Double sideband combined tracking
PLI	Phase lock indication
PLL	Phase locked loop
PSD	Power spectral density
SC	Side-peaks cancellation
SLL	Sub-carrier locked loop
SSB	Single-sideband
GNSS	Global Navigation Satellite Systems
PRN	Pseudo Random Noise
TOA	Time-of-arrival

Acknowledgements
Not applicable.

Author contributions
TF modeled double sideband combined tracking and its thermal noise. TZ proposed the structure of the double sideband combined tracking and guided the implementation and testing. HZ implemented structure of the double sideband combined tracking and verified it experimentally. JM guided modeling of double sideband combined tracking. XN guided manuscript writing. All authors read and approved the final manuscript.

Funding
This research is funded by the National Key Research and Development Program of China (No. 2020YFB0505803), and the National Natural Science Foundation of China (No. 41974024).

Availability of data and materials
Data sets generated during the current study are available from the corresponding author on reasonable request.

Declarations

Competing interests
The authors declare that they have no competing interests.

Received: 27 March 2023 Accepted: 7 August 2023
Published online: 16 October 2023

References

Betz, J. W., & Kolodziejski, K. R. (2009). Generalized theory of code tracking with an early-late discriminator part I: Lower bound and coherent processing. *IEEE Transactions on Aerospace and Electronic Systems, 45*(4), 1538–1556. https://doi.org/10.1109/TAES.2009.5310316

Borio, D. (2017). Coherent side-band BOC processing. *IET Radar, Sonar & Navigation, 11*(10), 1455–1466. https://doi.org/10.1049/iet-rsn.2016.0245

Burian, A., Lohan, E., & Renfors, M. (2006). BPSK-like methods for hybrid-search acquisition of galileo signals. *IEEE International Conference on Communications, 2006*, 5211–5216. https://doi.org/10.1109/ICC.2006.255493

Changlu, Q., Jing, L., & Yangzhi, L. (2010). Research of AltBOC modulation. In *2010 IEEE 12th international conference on communication technology* (pp. 925–929). https://doi.org/10.1109/ICCT.2010.5688541.

Chen, H., Wang, R., Jia, W., Ren, J., & Yao, M. (2013). An unambiguous tracking method based on pseudo correlation function for AltBOC(15,10) signal. *Wireless Personal Communications, 69*(4), 1347–1364. https://doi.org/10.1007/s11277-012-0637-z

De Wilde, W., Sleewaegen, J.-M., Van Wassenhove, K., & Wilms, F. (2004). A first-of-a-kind galileo receiver breadboard to demonstrate galileo tracking algorithms and performances. In *Proceedings of the 17th international technical meeting of the satellite division of the institute of navigation (ION GNSS 2004)* (pp. 2645–2654). http://www.ion.org/publications/abstract.cfm?jp=p&articleID=5948.

Diessongo, T. H., Schüler, T., & Junker, S. (2014). Precise position determination using a Galileo E5 single-frequency receiver. *GPS Solutions, 18*(1), 73–83. https://doi.org/10.1007/s10291-013-0311-2

European Union. (2021). *OS SIS ICD: Galileo Open service signal in space interface control document, Issue 2.0*. https://www.gsc-europa.eu/sites/default/files/sites/all/files/Galileo_OS_SIS_ICD_v2.0.pdf.

Feng, T., Kai, Z., & Liang, C. (2016). Unambiguous tracking of BOC signals using coherent combination of dual sidebands. *IEEE Communications Letters, 20*(8), 1555–1558. https://doi.org/10.1109/LCOMM.2016.2569520

Heiries, V., Roviras, D., Ries, L., & Calmettes, V. (2004). Analysis of non ambiguous BOC signal acquisition performance. In *Proceedings of the 17th international technical meeting of the satellite division of the institute of navigation (ION GNSS 2004)* (pp. 2611–2622). http://www.ion.org/publications/abstract.cfm?jp=p&articleID=5945.

Hodgart, M. S., & Blunt, P. D. (2007). Dual estimate receiver of binary offset carrier modulated signals for global navigation satellite systems. *Electronics Letters, 43*(16), 877. https://doi.org/10.1049/el:20071101

Hodgart, M. S., Blunt, P. D., & Unwin, M. (2007). The optimal dual estimate solution for robust tracking of binary offset carrier (BOC) modulation. In *Proceedings of the 20th international technical meeting of the satellite division of the institute of navigation (ION GNSS 2007)* (pp. 1017–1027). http://www.ion.org/publications/abstract.cfm?jp=p&articleID=7604.

Hodgart, M. S., & Simons, E. (2012). Improvements and additions to the double estimation technique. In *2012 6th ESA workshop on satellite navigation technologies (Navitec 2012) & European workshop on GNSS signals and signal processing* (pp. 1–7). https://doi.org/10.1109/NAVITEC.2012.6423053.

Kaplan, E. D., & Hegarty, C. (Eds.). (2017). *Understanding GPS/GNSS: Principles and applications* (3rd ed.). Artech House.

Kovár, P., Kacmarik, P., & Vejrazka, F. (2011). Interoperable GPS, GLONASS and Galileo software receiver. *IEEE Aerospace and Electronic Systems Magazine, 26*(4), 24–30. https://doi.org/10.1109/MAES.2011.5763340

Lee, Y., Lee, Y., Yoon, T., Song, C., Kim, S., & Yoon, S. (2009). AltBOC and CBOC correlation functions for GNSS signal synchronization. In *Computational science and its applications—ICCSA 2009, 5593* (pp. 325–334). https://doi.org/10.1007/978-3-642-02457-3_28.

Lestarquit, L., Artaud, G., & Issler, J.-L. (2008). AltBOC for dummies or everything you always wanted to know about AltBOC. In *Proceedings of the 21st international technical meeting of the satellite division of the institute of navigation (ION GNSS 2008)* (pp. 961–970). http://www.ion.org/publications/abstract.cfm?jp=p&articleID=8018.

Margaria, D., Dovis, F., & Mulassano, P. (2008). Galileo AltBOC signal multiresolution acquisition strategy. *IEEE Aerospace and Electronic Systems Magazine, 23*(11), 4–10. https://doi.org/10.1109/MAES.2008.4693984

Martin, N., Leblond, V., Guillotel, G., & Heiries, V. (2003). BOC(x,y) Signal acquisition techniques and performances. In *Proceedings of the 16th international technical meeting of the satellite division of the institute of navigation (ION GPS/GNSS 2003)* (pp. 188–198). http://www.ion.org/publications/abstract.cfm?jp=p&articleID=5194.

Mo, J., Zhang, T., & Niu, X. (2021). Getting to E5 with ease: An AltBOC double-sideband receiver based on single-sideband correlation. *Inside GNSS*. https://insidegnss.com/getting-to-e5-with-ease-an-altboc-double-sideband-receiver-based-on-single-sideband-correlation/.

Padokhin, A. M., Mylnikova, A. A., Yasyukevich, Y. V., Morozov, Y. V., Kurbatov, G. A., & Vesnin, A. M. (2021). Galileo E5 AltBOC signals: Application for single-frequency total electron content estimations. *Remote Sensing*, *13*(19), Article 19. https://doi.org/10.3390/rs13193973.

Prochniewicz, D., & Grzymala, M. (2021). Analysis of the impact of multipath on galileo system measurements. *Remote Sensing*, *13*(12), Article 12. https://doi.org/10.3390/rs13122295.

Rebeyrol, E., Julien, O., Macabiau, C., Ries, L., Delatour, A., & Lestarquit, L. (2007). Galileo civil signal modulations. *GPS Solutions, 11*(3), 159–171. https://doi.org/10.1007/s10291-006-0047-3

Ren, J., Jia, W., Chen, H., & Yao, M. (2012). Unambiguous tracking method for alternative binary offset carrier modulated signals based on dual estimate loop. *IEEE Communications Letters, 16*(11), 4.

Ren, J., Yang, G., Jia, W., & Yao, M. (2014). Unambiguous tracking method based on combined correlation functions for sine/cosine-BOC CBOC and AltBOC modulated signals. *Radioengineering, 23*(1), 244–251.

Shivaramaiah, N. C., & Dempster, A. G. (2008). An analysis of Galileo E5 acquisition strategies. In *European Navigation conference (ENC-GNSS)*. European Navigation Conference (ENC-GNSS).

Shivaramaiah, N. C., & Dempster, A. G. (2009a). A novel extended tracking range DLL for AltBOC signals. In *2009 IEEE 70th vehicular technology conference fall* (pp. 1–5). https://doi.org/10.1109/VETECF.2009.5379090.

Shivaramaiah, N. C., & Dempster, A. G. (2009b). The Galileo E5 AltBOC: Understanding the signal structure. In *International global navigation satellite systems society IGNSS symposium*.

Shivaramaiah, N. C., Dempster, A. G., & Rizos, C. (2009). Hybrid tracking loop architectures for the Galileo E5 signal. In *Proceedings of the European navigation conference on global navigation satellite systems ENC GNSS*.

Silva, P. F., Silva, J. S., Peres, T., Fernandez, A., Palomo, J. M., Andreotti, M., Hill, C., Colomina, I., Miranda, C., & Pares, M. E. (2012). Galileo AltBOC signal processing for precise positioning—Experimental results. In *Proceedings of the 25th international technical meeting of the satellite division of the institute of navigation (ION GNSS 2012)* (pp. 1126–1135). http://www.ion.org/publications/abstract.cfm?jp=p&articleID=10325.

Sleewaegen, J.-M., De Wilde, W., & Hollreiser, M. (2004). Galileo AltBOC receiver. In *Proceedings of ENC-GNSS-2004*, 9.

Sousa, F. M. G., & Nunes, F. D. (2013). New expressions for the autocorrelation function of BOC GNSS signals: New expressions for the ACF of BOC GNSS signals. *Navigation: Journal of the Institute of Navigation, 60*(1), 1–9. https://doi.org/10.1002/navi.30

Spilker Jr., J. J., Axelrad, P., Parkinson, B. W., & Enge, P. (1996). *Global positioning system: Theory and applications*. American Inst. of Aeronautics and Astronautics.

Wang, L., Huang, X., Li, J., Tang, X., & Wang, F. (2020). Proposal of spread spectrum MSK for BDS RDSS signal modulation. *IET Radar, Sonar & Navigation, 14*(6), 870–878. https://doi.org/10.1049/iet-rsn.2019.0533

Xiao, G., Li, P., Sui, L., Heck, B., & Schuh, H. (2018). Estimating and assessing Galileo satellite fractional cycle bias for PPP ambiguity resolution. *GPS Solutions, 23*(1), 3. https://doi.org/10.1007/s10291-018-0793-z

Xie, G. (2009). *Principles of GPS and receiver design* (7th ed.). Publishing House of Electronics Industry.

Yao, Z., Cui, X., Lu, M., Feng, Z., & Yang, J. (2010). Pseudo-correlation-function-based unambiguous tracking technique for sine-BOC signals. *IEEE Transactions on Aerospace and Electronic Systems, 46*(4), 1782–1796. https://doi.org/10.1109/TAES.2010.5595594

Yarlykov, M. S. (2016). Correlation functions of BOC and AltBOC signals as the inverse Fourier transforms of energy spectra. *Journal of Communications Technology and Electronics, 61*(8), 857–876. https://doi.org/10.1134/S1064226916080180

Ye, W., Fang, J., & Li, J. (2017). Intelligent identification and mitigation of GNSS multipath errors using adaptive BOCPD. *Aerospace Science and Technology, 70*, 453–460. https://doi.org/10.1016/j.ast.2017.08.028

Zhu, Y., Cui, X., & Lu, M. (2015). Dual binary phase-shift keying tracking method for Galileo E5 AltBOC(15,10) signal and its thermal noise performance. *IET Radar, Sonar & Navigation, 9*(6), 669–680. https://doi.org/10.1049/iet-rsn.2014.0349

Publisher's Note